Measured and Predicted Heating Distributions for Biconics at Mach 10

Charles G. Miller,* Peter A. Gnoffo,† and Sue E. Wilder‡
NASA Langley Research Center, Hampton, Virginia

Heating distributions were measured on a 1.9% scale model of a generic aeroassisted vehicle proposed for missions to a number of planets and for use as a moderate lift-to-drag Earth orbital transfer vehicle. This vehicle is a spherically blunted, 13 deg/7 deg biconic with the fore cone bent upward 7 deg to provide self-trim capability; also tested was a straight biconic with the same nose radius and half-angles. These measurements were made in the Langley 31-in. Mach 10 Tunnel at values of the freestream Reynolds number, based on model length, equal to 2 and 9×10^5. The angle of attack, referenced to the aft cone, was varied from 0 to 20 deg. Heating distributions predicted with a parabolized Navier-Stokes (PNS) code are compared to measurements for the present Reynolds numbers and range of angle of attack. Leeward heating was greatly affected by Reynolds number, with the heating increasing with decreasing Reynolds number for attached flow (low incidence). The opposite was true for separated flow, which occurred when the fore-cone angle of attack exceeded 0.8 times the forecone half-angle. Windward heating distributions were predicted to within 10% by the PNS code. Leeward heating distributions were predicted qualitatively for both values of Reynolds number, but quantitative agreement was poorer than on the windward side.

Nomenclature

C^* = $\mu^* T_\infty / \mu_\infty T^*$
C_h = heat-transfer coefficient, $= \dot{q}/(h_{t,2} - h_w)$, ℑ-s/m^4
h = enthalpy, ℑ/kg
L = length, m
M = Mach number
p = pressure, N/m^2
$\dot{q}$ = heat-transfer rate, W/m^2
$\dot{q}_{sph}$ = stagnation-point heat-transfer rate to a sphere, W/m^2
r = radius, m
R = unit Reynolds number, m^{-1}
St_∞ = Stanton number, $C_h/\rho_\infty U_\infty$
t = time, s
T = temperature, K
T^* = reference temperature, $= (T_{t,2}/6)(1+3T_w/T_{t,2})$, K
$\bar{v}^*$ = viscous interaction parameter, $= M_\infty (C^*/R_{\infty,L})^{1/2}$
x,y,z = model coordinates, m (see Fig. 1)
α = angle of attack, deg
μ^* = viscosity evaluated at T^*, N-s/m^2
η = nose bend angle, deg
θ = cone half-angle, deg
ρ = density, kg/m^3
ϕ = circumferential angle measured from the most leeward meridian, deg

Subscripts

a,f = aft- and fore-cone sections, respectively
e = effective
i = isothermal ($T_w = 300$ K)
n = nose
sph = sphere
$t,1$ = reservoir conditions
$t,2$ = stagnation conditions behind normal shock
w = model surface
2 = static conditions immediately behind normal shock
∞ = freestream conditions

Received Sept. 13, 1984; revision received Sept. 12, 1985.

*Aero-Space Engineer, Experimental Aerodynamics Branch, Space Systems Division. Senior Member AIAA.
†Aero-Space Engineer, Aerothermodynamics Branch, Space Systems Division. Member AIAA.
‡Aero-Space Technologist, Aerothermodynamics Branch, Space Systems Division. Retired.

Introduction

AREKINDLING of interest in aerobraking and aerocapture techniques for planetary missions[1,2] and Earth orbital transfer vehicles (OTV)[3] has occurred in recent years. A generic vehicle proposed for missions to a number of planets[1,2] and a moderate lift-to-drag OTV candidate, which also offers advantages as a re-entry vehicle, is a spherically blunted biconic with the fore-cone section bent upward relative to the aft-cone section to provide self-trim capability. Because of the scarcity of experimental data for bent biconics, a study was initiated at the NASA Langley Research Center to establish a comprehensive data-base for this vehicle. Aerodynamic coefficients, pressure distributions, oil-flow patterns, and shock shapes have been measured on 2.9% scale models of the proposed configuration and on models without a bent nose (straight biconic) but with the same nose radius, base radius, and half-angles.[4-6] These measurements were made in three conventional (as opposed to impulse) hypersonic wind tunnels, namely, the 20-in. Mach 6 Tunnel, the 31-in. Mach 10 Tunnel (formerly known as the Continuous Flow Hypersonic Tunnel), and the Hypersonic CF_4 Tunnel, to provide a range of Mach number, Reynolds number, and ratio of specific heats. More recently, heating distributions were measured on 1.9% scale models in the Langley Expansion Tube, an impulse facility, at hypersonic-hypervelocity flow conditions for four test gases.[7]

As part of the overall program to establish a data-base for this generic aeroassisted vehicle, a study was performed to examine the effect of nose bend, angle of attack, and Reynolds number on longitudinal heating distributions. Heating distributions were measured on a 1.9% scale model of this vehicle in the Langley 31-in. Mach 10 Tunnel; also tested was a straight biconic with the same nose radius, base radius, and half-angles. The purpose of this paper is threefold: 1) to illustrate the effect of nose bend, angle of attack, and Reynolds number on heating at Mach 10 in air; 2) to compare heating distributions predicted with a code,[8] which solves the three-dimensional parabolized Navier-Stokes equations, to measurements over an angle-of-attack range; and 3) to compare the present hypersonic ideal-air results to the hypersonic-

hypervelocity real (dissociated) air heating distributions measured on these same models in the Langley Expansion Tube.[7] (It should be noted that the present study is the first at Langley to use a model with a large number of thin-film resistance heat-transfer gages[9] in a conventional hypersonic wind tunnel.)

Experimental Method

Facility

The Langley 31-in. Mach 10 Tunnel[10] uses a water-cooled, three-dimensional contoured nozzle to generate a nominal Mach number of 10 with dry air as the test gas. The test section is 78.7 cm square, the maximum operating reservoir pressure is 15.2 MPa, and the maximum reservoir temperature is 1060 K. This facility was operated in the blowdown mode for the present study and will be referred to herein as the Mach 10 Tunnel.

Models

A sketch and dimensions of the biconic models tested in Ref. 7 and in the present study are shown in Fig. 1. The bent-biconic model represents a 1.9% scale of the proposed Mars sample return, single-mission vehicle.[1] The models were fabricated from stainless steel, and each model contained five slots for instrumented inserts. Two slots were machined along the most windward ray ($\phi = 180$ deg) (one on the fore cone and one on the aft cone), two along the most leeward ray ($\phi = 0$ deg), and one 90 deg between the most windward and leeward rays on the aft cone. The models were supported by a 35.6-cm-long, 1.9-cm-diam sting.

Instrumentation

The thin-film heat-transfer gage technology developed for the Langley Expansion Tube[7,9] was used without change in the present tests. Use of the same gages in facilities with very different run times (2×10^{-4} s for the Langely Expansion Tube and 2 s for the Mach 10 Tunnel) was possible because the relatively large width (6.4 mm) and thickness (5.1 mm) of the substrates provided one-dimensional behavior[9] in both facilities. The substrates were fabricated from MACOR,§ a machinable glass-ceramic, and contoured to the conic section. Eight palladium gages, each approximately 1000 Å thick, were deposited on the polished surface of each substrate. The nose section was fabricated from MACOR and a single thin-film gage located at the spherical tip. All gages were in the form of a serpentine pattern[9] and provided nearly a point measurement since the sensing surface was 1 × 1.3 mm. Details of gage construction and calibration are discussed in Ref. 9.

A portable data-acquisition system consisting of 100 channels of constant-current circuitry was used in this study. Each channel (circuit) had a differential amplifier allowing a gain selection from 1 to 100 and a constant-current selection of either 1 or 4 mA. These circuits were wired to a 12-bit, 104-channel, analog-to-digital (A/D) data-acquisition system that samples each channel at a rate of 50 times/s; the extra four channels were used to monitor tunnel parameters. This A/D system was interfaced to a desktop computer. The 100-channel system is self-calibrating (100-Ω precision resistors were switched into each circuit, the voltage measured, and the current computed), and the initial voltage across each gage was recorded by the computer just minutes prior to the run.

Oil-flow tests were performed with larger (2.9% scale) models fabricated for force and moment tests.[5,6] These models were painted black and sprayed with a mixture of white artist's oil pigment and silicon oils of various viscosities. The model was rapidly injected into the flow, retracted, removed from the facility, and the flow patterns photographed.

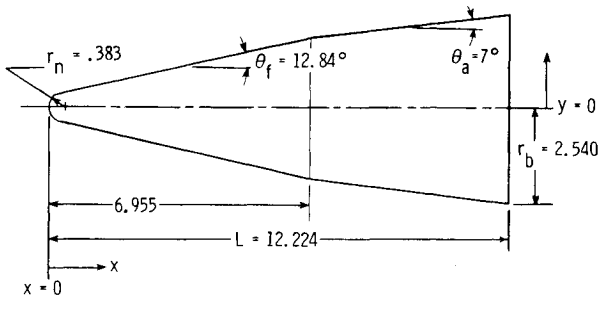

a) Straight biconic.

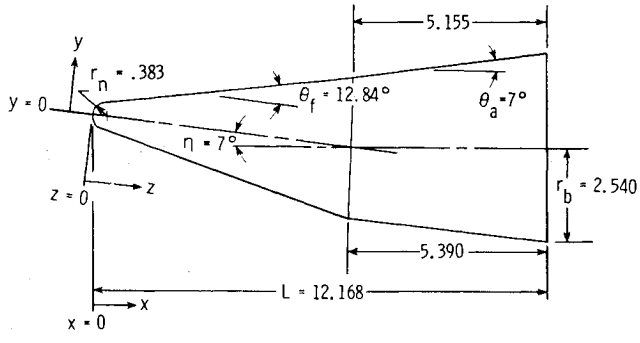

b) Bent biconic.

Fig. 1 Sketch and dimensions of models. (All dimensions in cm.)

Test Conditions

Nominal reservoir conditions and corresponding freestream flow parameters for the present study are presented in Table 1. Both biconic models were tested over an angle-of-attack range from 0 to 20 deg in 2- or 4-deg increments at each flow condition. The angle of attack is referenced to the axis of the aft-cone section.

Data Reduction

The numerical method used to compute values of the heat-transfer rate from the output of the thin-film resistance gages is discussed in Ref. 9. Present values of $\dot{q}$ are based on a more accurate determination of the thermal properties of MACOR[7] than that presented in Ref. 9, and account for the variation of substrate thermal properties with temperature. The heat-transfer coefficient was essentially constant for the time interval $0.5 \leq t < 1.5$ s for all gages and runs. ($t = 0$ is defined as the time the model first experiences an increase in surface temperature as it is inserted into the flow from a sheltered position.) Values of $\dot{q}$ (or C_h) presented herein correspond to $t = 1$ s.

To eliminate time as a variable, the present heating data are plotted in terms of the heat-transfer coefficient $C_h = \dot{q}(t)/[h_{t,2} - h_w(t)]$. These values of C_h are nondimensionalized by the heat-transfer coefficient $C_{h,\mathrm{sph}}$ obtained from the stagnation-point heat-transfer rate of a sphere $\dot{q}_{\mathrm{sph}}$ with its radius equal to the biconic nose radius. This value of $C_{h,\mathrm{sph}}$ is computed by using the theory of Fay and Riddell[11] with $T_w = 300$ K. Comparisons between prediction and measurement are made in terms of the heat-transfer rate for an isothermal ($T_w = 300$ K) model. Nominal values of predicted $\dot{q}_{\mathrm{sph}}$ and $C_{h,\mathrm{sph}}$ are given in Table 1.

Uncertainties

Probable sources of error for thin-film resistance gages are discussed in Refs. 7 and 9. It is worthy of note that calibra-

§Trade name for Corning Glass Works Code 9658.

Table 1 Nominal flow conditions

$p_{t,1}$, MPa	$T_{t,1}$, K	p_∞, Pa	T_∞, K	M_∞	$R_{\infty,L}$, $\times 10^5$	$\dot{q}_{\text{sph}}$, MW/m^2	$C_{h,\text{sph}}$, J-s/m^4
2.4	980	61	49.8	9.9	2.2	0.328	0.451
10.9	1005	227	48.4	10.2	9.3	0.680	0.905

Note: The value of L used to determine $R_{\infty,L}$ is 12.2 cm. Values of $\dot{q}_{\text{sph}}$ and $C_{h,\text{sph}}$ were computed using the theory of Fay-Riddell[11] for $r_n = 3.83$ mm and $T_w = 300$ K.

tions performed before and immediately after the present test series revealed that the temperature coefficient of resistance was stable for all gages on the aft cone to within 0.2% for both models. Agreement between pre- and post-test calibrations was poorer for gages on the fore cone, but was still within 1.2%. The heat-transfer rate inferred from the present thin-film gages is believed accurate to within ±5%. Run-to-run repeatability was excellent; for example, the agreement in $C_h/C_{h,\text{sph}}$ between repeat runs was within 1% for all but a few gages.

Prediction Method

Heating distributions were computed using a computer code that solves the steady, three-dimensional parabolized Navier-Stokes (PNS) equations.[12,13] This code requires supersonic flow in the downstream marching direction from the starting data plane at or in front of the sphere-cone junction. The starting data plane is determined from the Navier-Stokes solution over a sphere using a finite-volume, adaptive-grid algorithm.[14] The PNS code of Refs. 12 and 13 has been modified to include the straight biconic and bent-nose biconic geometries, and increased circumferential resolution was added;[8] also added was the capability to compute equilibrium real-gas effects of the C, H, He, O, and N systems. The differences in predicted values of heat-transfer rate for ideal and real air in thermochemical equilibrium, which includes vibrational excitation, were insignificant for the present models and flow conditions. This PNS code was run successfully for angles of attack from 0 to 20 deg. All predictions presented herein are for laminar flow.

Results and Discussion

Before presenting the data that illustrate the effects of nose bend, freestream Reynolds number, and angle of attack on longitudinal heating distributions, oil-flow patterns illustrating the influence of angle of attack and Reynolds number on leeward surface flow characteristics are presented. These are presented prior to the heating distributions to reveal certain aspects of the leeward flow that may not be inferred from the heating measurements alone. The last two sections present comparisons of the data of this study with predictions from the PNS code[8] and with the real-air data obtained in the Expansion Tube.[7]

Leeward Surface Oil-Flow Patterns

A diagnostic tool that provides information on surface streamlines and thus reveals the complexity of the leeward flow for these biconics at incidence is surface oil-flow patterns. The effect of angle of attack and Reynolds number at Mach 10 on leeward oil-flow patterns for the bent biconic is shown in Fig. 2. For $R_{\infty,L} = 1.3 \times 10^6$, the flow is attached at zero incidence but separates as α is increased to 5 deg (Figs. 2a and 2b; that is, as the fore-cone angle of attack α_f approaches the fore-cone half-angle θ_f). The separation region moves upstream with increasing α and is near the nose at $\alpha = 20$ deg. Comparison of Figs. 2c and 2d illustrates a strong influence of Reynolds number on leeward surface flow characteristics. An increase in Reynolds number promoted flow separation and caused the primary vortex to split and form a secondary vortex.

Typical of blunt cones at incidence,[15] a large, favorable pressure gradient exists on the leeward side just downstream

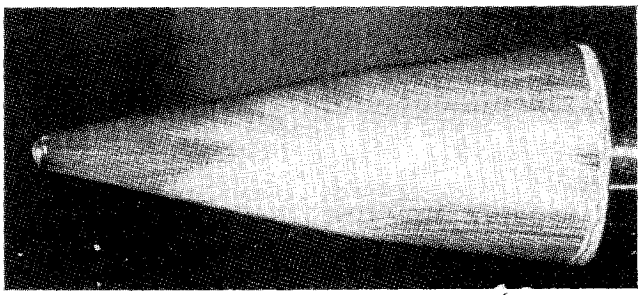

a) $\alpha = 0$ deg, $M_\infty = 10.2$, $R_{\infty,L} \approx 1.3 \times 10^6$.

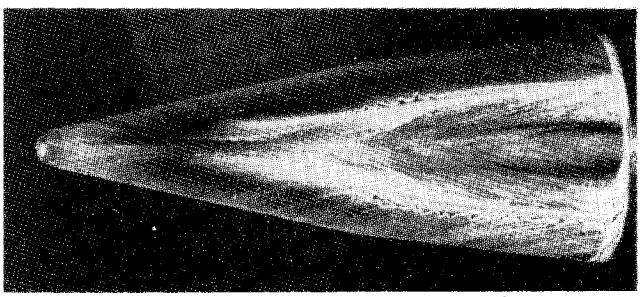

b) $\alpha = 5$ deg, $M_\infty = 10.2$, $R_{\infty,L} \approx 1.3 \times 10^6$.

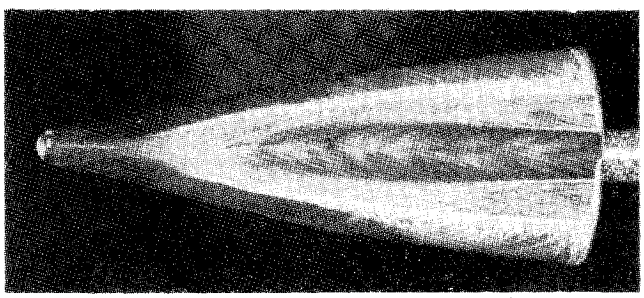

c) $\alpha = 10$ deg, $M_\infty = 10.2$, $R_{\infty,L} \approx 1.3 \times 10^6$.

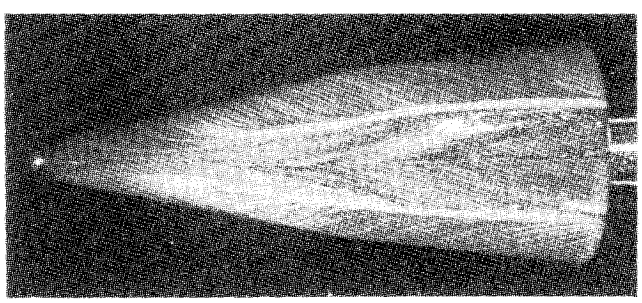

d) $\alpha = 10$ deg, $M_\infty = 9.9$, $R_{\infty,L} \approx 3 \times 10^5$.

Fig. 2 Effect of angle of attack and Reynolds number on leeward surface oil-flow patterns for bent biconic.

of the nose causing the boundary layer to remain attached. In this region close to the nose, the lateral component of skin friction is in the direction of the most leeward ray; however, at larger distances downstream of the nose, the lateral component changes direction and is now away from the most leeward ray. When this change in direction occurs, two symmetrical separation lines develop just downstream of the region where the lateral component of skin friction passes through zero. The longitudinal component of skin friction in the vicinity of the most leeward ray is finite, as revealed by oil that flowed

from the attached region just downstream of the nose, through the region of zero lateral skin friction, and into the vortex region.

Effect of Nose Bend

Longitudinal heating distributions for the bent biconic are compared with those for the straight biconic in Fig. 3 for two angles of attack at the lower value of Reynolds number. As mentioned previously, the angle of attack is referenced to the aft-cone section of both models; that is, the effect of nose bend is examined by holding the aft section fixed at a given angle of attack and bending the fore cone upward 7 deg. Naturally, at the lower angles of attack, higher heating along the most windward ray ($\phi = 180$ deg) and lower heating along the most leeward ray ($\phi = 0$ deg) of the fore cone occur for the bent biconic; however, because of the larger expansion at the fore-cone/aft-cone junction for the bent biconic, a decrease in the windward aft-cone heating occurs. At zero incidence, heating along the most windward ray of the aft cone was actually less than along the midmeridian ($\phi = 90$ deg) ray for the bent biconic. This trend is in qualitative agreement with measured pressure distributions[4] at Mach 6, which revealed that the pressure along the midmeridian ray of the bent biconic aft cone at $\alpha = 0$ deg exceeded the pressure along the windward ray by 5-10%. The heating along these two rays on the aft cone is essentially the same at $\alpha = 4$ deg (Fig. 3a), which does not follow the pressure distribution[4] at Mach 6 (pressure along the $\phi = 180$ deg ray exceeds that along the $\phi = 90$ deg ray). It is not until $\alpha \geq 8$ deg (Fig. 3b) that the heating along the windward ray exceeds that along the midmeridian ray.

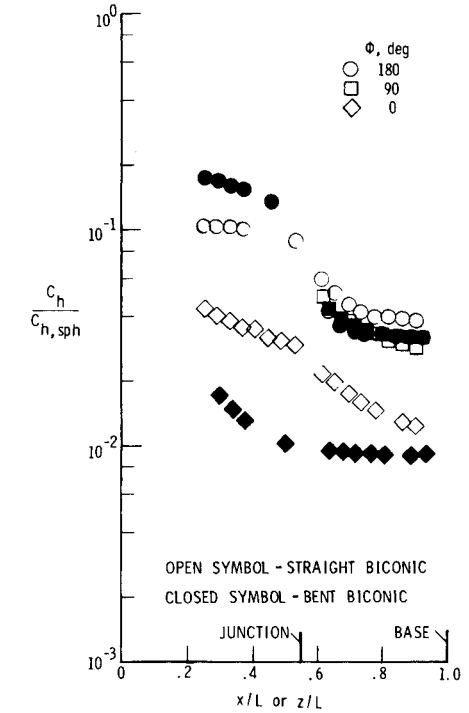

a) $\alpha = 4$ deg.

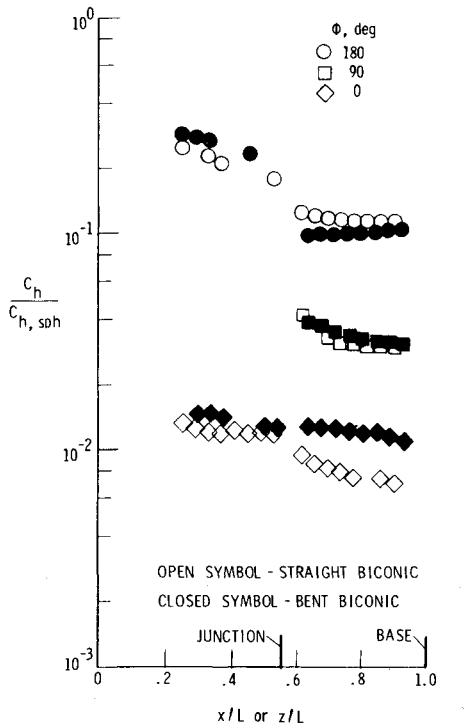

b) $\alpha = 20$ deg.

Fig. 3 Longitudinal heating distributions for straight and bent biconics at angles at attack. $M_\infty = 9.9$, $R_{\infty,L} \approx 2.2 \times 10^5$.

Another interesting trend observed in Fig. 3 is the crossing and trend reversal of the leeward heating distributions for the two biconics as the angle of attack is increased. The nose bend results in a lower leeward heating at the lower angles of attack but a higher heating at the higher angles of attack. This crossing and trend reversal may possibly be attributed to the nose bend causing an earlier circumferential separation of the flow on the leeward side for a given angle of attack or, possibly, to an earlier transition from laminar to turbulent flow. Now, the oil-flow patterns revealed that the leeward flow for the straight biconic remains attached for 0 deg $\leq \alpha \leq 8$ deg, whereas circumferential flow separation is expected for the bent biconic or $\alpha > 4$ deg; thus, the lower leeward heating for the bent biconic at $\alpha = 0$ and 4 deg is expected. At $\alpha = 8$ deg, the circumferential flow separation that occurs for the bent biconic results in the formation of longitudinal, counter-rotating primary vortices that reattach along the most leeward ray, thereby forming a "stagnation line" and augmenting the heating along this ray. From the oil-flow patterns, the flow separation originates just upstream of the base and moves upstream with increasing angle of attack, which is expected to cause a forward movement of the augmented leeward heating. Hence, the leeward heating distributions in Fig. 3 are consistent with the oil-flow patterns.

The fact that circumferential flow separation occurred is known from the oil-flow patterns; what is unknown is whether the separated flow remained laminar or became transitional. There is general agreement in the literature that the transition location for blunt cones moves forward on the leeward ray with increasing angle of attack (see, for example, Ref. 16). Because both circumferential flow separation and transition cause an increase in leeward heating and produce the same trends with angle of attack (forward movement with increasing α), there is a problem distinguishing the effects of these two phenomena. The primary contributor to the trends in leeward heating observed in Fig. 3 is believed to be flow separation due to the following: 1) the consistency between the oil-flow patterns and heating distributions, and 2) the qualitative agreement between measurement and laminar flow predictions, to be discussed subsequently in the subsection "Comparison of Prediction to Measurement." This is not to imply that transition did not occur in the separated flow region (vortex system); however, whether or not transition occurred for the conditions of this study is unknown.

The windward heating for the bent biconic at a given angle of attack is nondimensionalized by the windward heating for the straight biconic at the same α and is presented in Fig. 4 for the higher value of Reynolds number. The increase in windward fore-cone heating due to the nose bend diminishes rapidly with increasing angle of attack (as expected) and is only about 20% at $\alpha = 20$ deg (design trim angle of attack for bent biconic[1,2]). The decrease in windward aft-cone heating caused

by the nose bend is clearly illustrated in Fig. 4, and should also be of interest to the designer sizing the thermal protection system for such a vehicle because the aft-cone surface area represents roughly 60% of the total surface area. Contrary to the fore-cone heating, this ratio (bent to straight) on the aft cone is not strongly influenced by the angle of attack. The windward aft-cone heating levels for the two biconics approach one another with distance downstream of the fore-cone/aft-cone junction; that is, the effect of the nose bend on windward aft-cone heating diminishes with distance downstream from the junction and is less than 10% just ahead of the base for these biconics.

Effect of Reynolds Number

The effect of Reynolds number on heating distributions for the straight biconic is shown in Fig. 5. No effect of Reynolds number on windward fore-cone heating was observed on either biconic over the present range of angle of attack; this was also the case for a 15.1 deg/11.3 deg straight biconic tested at these same conditions in the Mach 10 Tunnel.[17] A small but distinguishable effect of Reynolds number on windward aft-cone heating was observed. However, the variation in heating between the two values of Reynolds number is generally within the experimental uncertainty, thereby precluding a definite conclusion that the aft-cone windward heating is dependent on $R_{\infty,L}$ for $\alpha \leq 16$ deg and independent of $R_{\infty,L}$ at $\alpha = 20$ deg. In general, heating along the midmeridian ray increased slightly with decreasing $R_{\infty,L}$ over the present range of α for both biconics.

Unlike the windward side, a large effect of $R_{\infty,L}$ is observed on the leeward heating. For the straight biconic at $\alpha = 4$ deg (Fig. 5a) and 8 deg and for the bent biconic at $\alpha = 0$ deg, a significant increase in heating occurred as the Reynolds number was decreased. This increase in leeward heating with decreasing Reynolds number for attached flow may be primarily due to a significant increase in the boundary-layer displacement thickness with decreasing $R_{\infty,L}$.[18] The larger displacement thickness causes a larger induced surface pressure and heating level. Another possible contributor to this difference in leeward heating is vorticity interaction resulting from the boundary-layer thickening and interacting with the inviscid flow.[18] As the angle of attack is increased, the leeward heating distributions for the two values of $R_{\infty,L}$ cross one another. This crossing is the result of an increase in leeward heating (at the higher Reynolds number) that first occurs on the aft cone near the base and moves upstream with increasing angle of attack. For $\alpha_f > 16$ deg, an opposite variation in leeward heating with $R_{\infty,L}$ is observed for x/L or $z/L > 0.2$; the leeward heating now increases with increasing

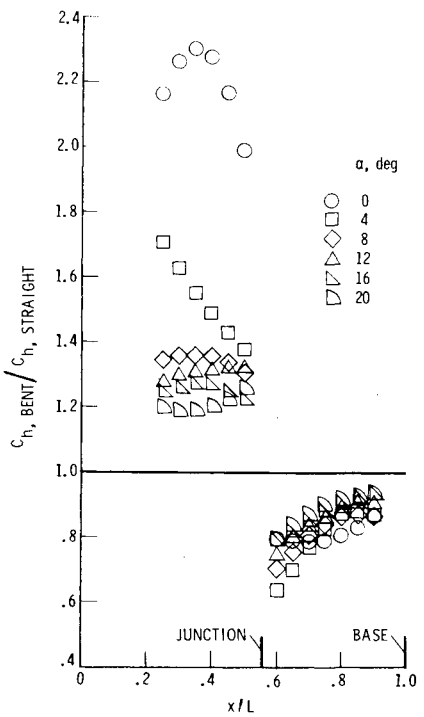

Fig. 4 Ratio of windward heat-transfer coefficient for bent biconic to that for a straight biconic at various angles of attack. $M_\infty = 10.2$, $R_{\infty,L} \approx 9.3 \times 10^5$.

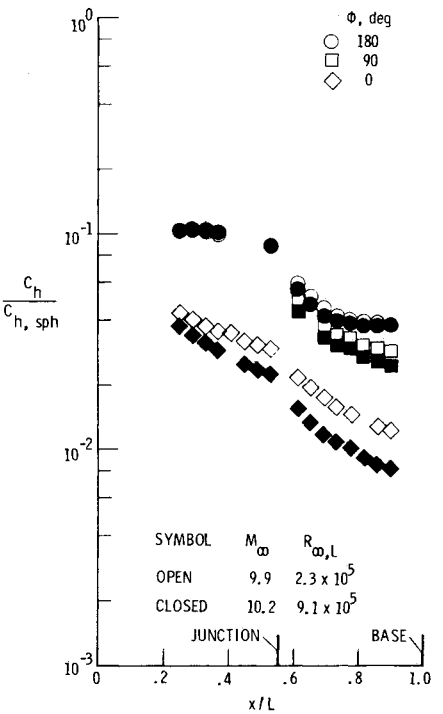

a) $\alpha = 4$ deg.

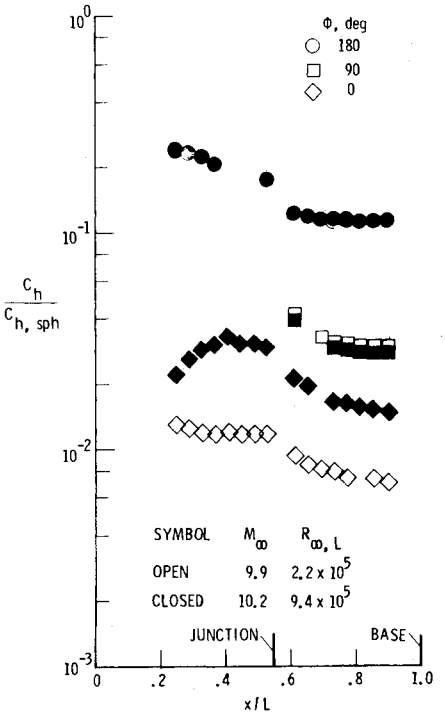

b) $\alpha = 20$ deg.

Fig. 5 Effect of Reynolds number on longitudinal heating distribution for a straight biconic.

$R_{\infty,L}$, as was also observed in Ref. 17. The trends of leeward heating are consistent with the oil-flow patterns, which show that for a given α an increase in Reynolds number will cause the flow to separate, thereby augmenting the leeward heating. The longitudinal leeward heating distributions at the highest value of $R_{\infty,L}$ also resemble those expected for transition from laminar to turbulent flow. Again, this is not to imply that transitional or turbulent flow on the leeward side necessarily occurred. Based on the present longitudinal heating distributions along the most windward ray ($\phi = 180$ deg) and along the midmeridian ray ($\phi = 90$ deg), which give no indication of transitional flow, and on previous studies in the Mach 10 Tunnel, transition on these relatively small, smooth models is not expected for attached flow; however, as discussed in the previous section, the possibility that transition occurs on the leeward side at angles of attack sufficiently large to cause circumferential flow separation may exist.

Effect of Angle of Attack

Heating to the most windward ray increased orderly with angle of attack for both biconics. The aft-cone windward heating for the biconics varied linearly with angle of attack, as did the fore-cone windward heating for the bent biconic at $\alpha > 0$ deg and the straight biconic at $\alpha > 4$ deg. Heating along the midmeridian ray of the aft cone of both biconics was nearly independent of angle of attack over the present range, which is typical of cones.[19]

The variation of leeward heating with angle of attack was not as orderly (i.e., increase only or decrease only with α) as that for the most windward and midmeridian rays. The influence of $R_{\infty,L}$ on leeward heating adds to this disorder. Leeward heating initially decreased with increasing angle of attack but reached a point where it then increased with a further increase in α, which is indicative of circumferential flow separation and possible transition. The heating distributions indicated that flow separation on the leeward side first occurred just upstream of the base and moved upstream as the angle of attack increased, as observed in the oil-flow tests. For the straight biconic at the lower Reynolds number, the angle of attack was varied in 2-deg increments. These results showed that leeward flow separation occurred when the fore-cone angle of attack exceeded 0.8 times the fore-cone half-angle. The sensitivity of leeward heating to angle of attack at a given value of x/L or z/L on the fore- and aft-cone sections is shown in Fig. 6 for both biconics. When presented in this manner, the angle of attack at which separation occurs on the aft cone becomes apparent. For example, for the straight biconic, the minimum aft-cone heating at $x/L = 0.78$ occurred at $\alpha = 12$ deg for the lower Reynolds number (Fig. 6) and at $\alpha = 8$ deg for the higher Reynolds number. Similarly, leeward flow separation on the aft cone of the bent biconic appeared to occur at around $\alpha = 4$ deg at the lower Reynolds number (Fig. 6) and at $\alpha = 0$ deg for the higher Reynolds number. Thus, an increase in Reynolds number caused separation to occur at a lower angle of attack.

Comparison of Prediction to Measurement

Heating distributions predicted with the PNS code are compared with measurements for the most windward and most leeward rays of the bent biconic in Fig. 7 for both Reynolds numbers. Both the measured and predicted results correspond to a model surface temperature of 300 K. In general, the PNS code slightly underpredicts heating on the fore cone, but is within 10%. On the leeward side, the agreement between prediction and measurement is poorer. The PNS code underpredicts heating up to 25% at the lower angles of attack, but the agreement improves at $\alpha \geq 16$ deg. The different trends in measured leeward heating distributions, due to the Reynolds number, are qualitatively predicted by the PNS code. Since this code was exercised only for laminar flow, this qualitative agreement implies the leeward flow prior to separation is laminar for both values of Reynolds number. One possible explanation for the PNS code tending to underpredict measured heating is that this code does not account for downstream influences propagating upstream through the subsonic portion of the boundary layer. There is evidence[20] that failure to include this effect will yield values of heating that are too low. Another possible contributor to the differences observed in leeward heating is that the separated leeward flow may be subjected to transitional flow effects at or prior to flow reattachment. All things considered, the PNS code provides a reasonably accurate prediction of the heating distributions on the present biconics in Mach 10 air for $0 \text{ deg} \leq \alpha \leq 20$ deg.

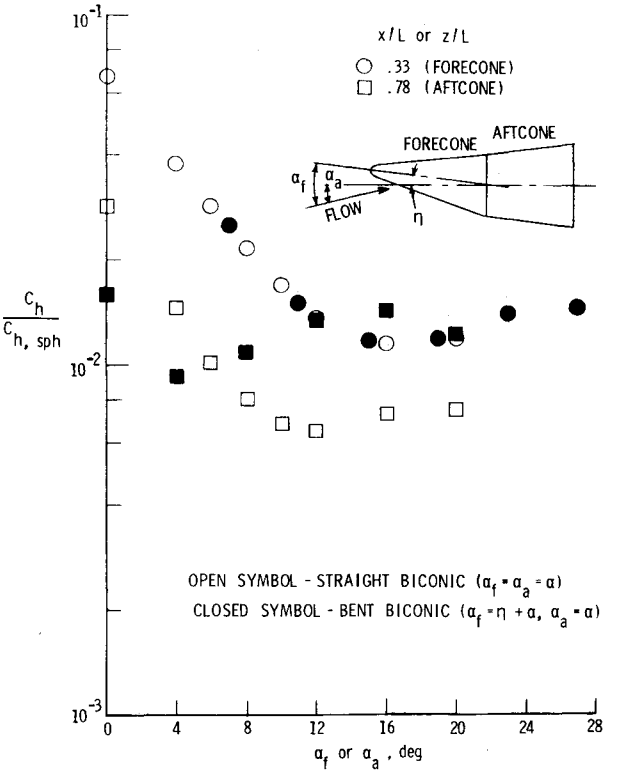

Fig. 6 Effect of angle of attack on leeward heating. $M_\infty = 9.9$, $R_{\infty,L} \approx 2.2 \times 10^5$.

Comparison of Ideal- and Real-Air Heating

The present results provide the opportunity to compare heating distributions measured in two distinctly different facilities—a hypervelocity-hypersonic impulse facility (Expansion Tube) and a conventional-type hypersonic wind tunnel (Mach 10 Tunnel)—with the same models and model instrumentation. Samples of such comparisons are shown in Fig. 8 for the bent biconic at $\alpha = 0$ and 20 deg. Heating distributions on the biconics (in terms of $C_h/C_{h,\text{sph}}$) measured in the Expansion Tube exceeded those measured in the Mach 10 Tunnel at the lower Reynolds number ($R_{\infty,L} = 2.2 \times 10^5$) over the present range of angles of attack. This was true for both the windward and leeward rays. Higher windward heating is expected for a real gas; however, the measured differences, which typically ranged from 20 to 35%, are significantly higher than those usually associated with real-gas effects alone (see, for example, Ref. 21).

Several factors are expected to contribute to the differences observed between the ideal-air Mach 10 Tunnel results and the real-air Expansion Tube results. One is the ratio of wall temperature to total temperature. Although the substrate surface temperatures at 200 μs in the Expansion Tube and at 1 s in the Mach 10 Tunnel were nearly the same, the Expansion Tube data correspond to a relatively low value of $T_w/T_{t,2}$ (0.05 as compared to 0.3 in the Mach 10 Tunnel), a fact that is expected to increase the heat-transfer rate. A second factor is viscous effects. Larger viscous effects are expected for the Ex-

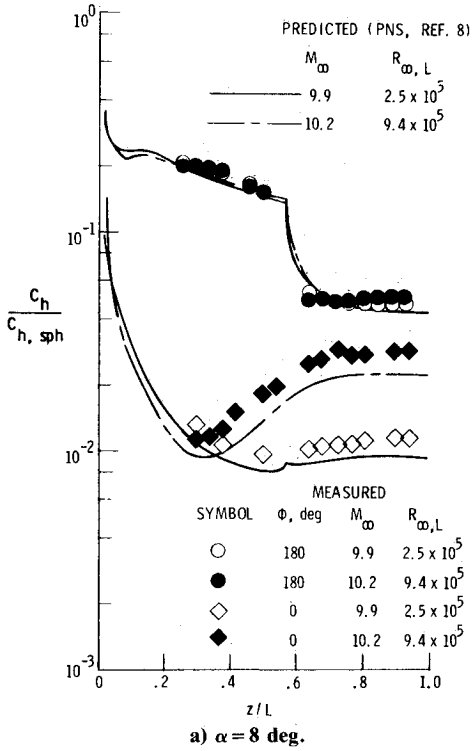

a) $\alpha = 8$ deg.

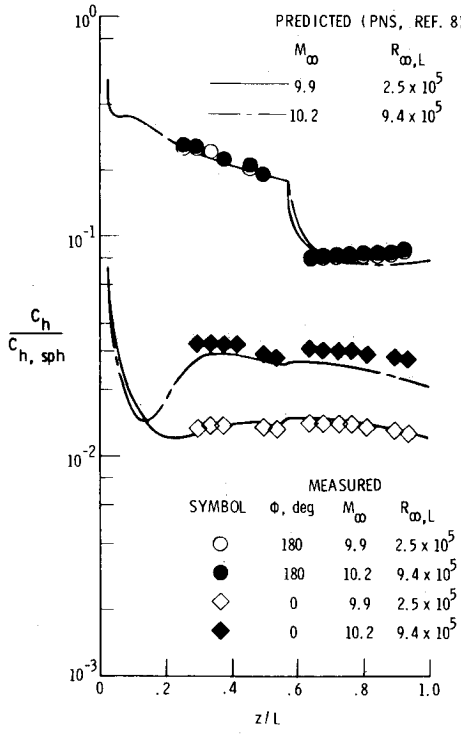

b) $\alpha = 16$ deg.

Fig. 7 Comparison of measured and predicted longitudinal heating distributions for a bent biconic at angles of attack.

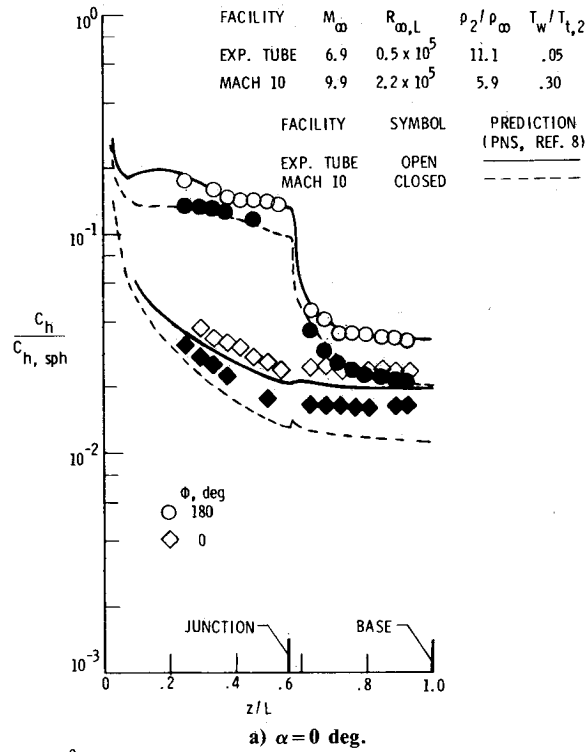

a) $\alpha = 0$ deg.

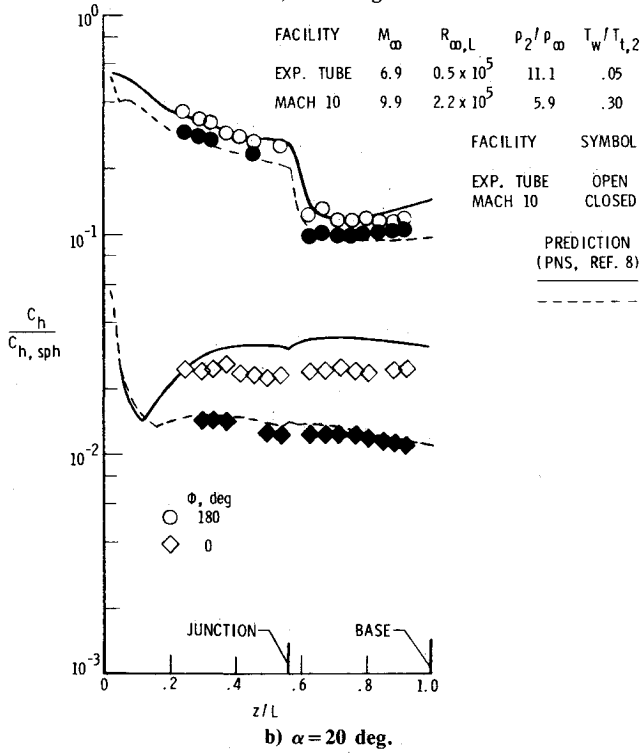

b) $\alpha = 20$ deg.

Fig. 8 Comparison of longitudinal heating distributions on a bent biconic measured in ideal air (Mach 10 Tunnel) and real air (Expansion Tube).[7]

pansion Tube results because of the lower Reynolds number, even though the lower value of $T_w/T_{t,2}$ may reduce these effects somewhat. Where the flow is attached, the most significant effect is probably induced heating due to the boundary-layer displacement thickness. Another effect that may contribute to the differences in Fig. 8 is external vorticity. The effect of external vorticity is expected to be more significant for the Expansion Tube results because of the greater shock strength (higher density ratio). A third factor is entropy-layer swallowing. The higher density ratio of the Expansion Tube causes a decrease in the shock detachment distance as compared with that in the Mach 10 Tunnel. Thus, the entropy layer is expected to be swallowed much quicker in the Expansion Tube tests, and the lower Reynolds number of the Expansion Tube flow accelerates this swallowing. The larger differences (35% to over a factor of 2) in leeward heating between the two facilities, as compared to windward heating, are expected because of the strong influence of Reynolds number on leeward heating.

Heating distributions predicted with the PNS code[8] for the ideal-air flow conditions of the Mach 10 Tunnel and the real-air flow conditions of the Expansion Tube are also shown in Fig. 8. The agreement in windward heating between measurement and prediction is relatively good at $\alpha = 0$

and 20 deg for both flow conditions; that is, the PNS code satisfactorily accounts for the differences in freestream flow conditions, shock strength (post-shock flow conditions), and wall temperature ratio on windward heating. Measured leeward heating at $\alpha = 0$ deg is underpredicted by the PNS code for both flow conditions; however, the differences between the predictions for the two flow conditions are about the same as the differences between the measurements over most of the length of the model. At $\alpha = 20$ deg, the PNS code predicts leeward heating for ideal air reasonably well, but overpredicts leeward heating for real air; thus, the code does not adequately account for the differences in flow conditions on leeward heating at this larger angle of attack.

Because of combined real-gas effects, which result in high-density ratios and may include nonequilibrium (or frozen) flow effects, viscous effects, and high wall cooling for the Expansion Tube results, it is difficult to determine the major contributors to the differences observed in Fig. 8. It should be noted, however, that the windward heating on these biconics in the hypervelocity helium flow, which behaved ideally, and hypervelocity air and nitrogen flows of the Expansion Tube[7] were correlated to within 10% for $\alpha > 4$ deg with an expression in the form

$$St_\infty \alpha \frac{\bar{v}^* \sin\theta_e}{(\rho_2/\rho_\infty)^{1/4}}$$

This proportionality shows that the windward heating for the conditions of the Expansion Tube tests is expected to be 30% higher than for the Mach 10 Tunnel tests at the lower Reynolds number, which is close to the differences observed in Fig. 8. The quantity $St_\infty (\rho_2/\rho_\infty)^{1/4}/v^*$ was observed to provide a reasonable correlation of the ideal- and real-air windward heating for the biconics. Thus, this proportionality may provide an approximate determination of real-air effects on windward heating for biconics from data obtained in hypersonic ideal-air wind tunnels.

Concluding Remarks

Laminar heating distributions were measured on a 1.9% scale model of a generic aeroassisted vehicle represented by a spherically blunted, 13 deg/7 deg biconic with the fore-cone section bent upward 7 deg to provide self-trim capability at a 20-deg angle of attack; also tested was a straight biconic (i.e., without a nose bend). Heating distributions were measured along the most windward, most leeward, and midmeridian rays of the biconic models in the Langley 31-in. Mach 10 Tunnel at values of the freestream Reynolds number based on model length of about 2 and 9×10^5. The angle of attack, referenced to the aft cone, was varied from 0 to 20 deg.

With the aft-cone section as the reference for angle of attack, the penalty (increase) in windward fore-cone heating due to the nose bend decreased with increasing angle of attack (as expected) and was only 20% at the design trim angle. This nose bend caused a decrease in windward aft-cone heating which is significant since the aft cone represents approximately 60% of the vehicle surface. No effect of Reynolds number on heating was observed on the windward side of the fore cone (although a small effect may have occurred on the aft cone). Quite the opposite was true on the leeward side, where an increase in Reynolds number caused circumferential flow separation to occur at a lower angle of attack. This influence of Reynolds number on flow separation was also illustrated by leeward surface oil-flow patterns, which revealed the existence of a primary vortex at the lower Reynolds number but primary and secondary vortices at the higher Reynolds number. For the case of attached flow (i.e., at low angles of attack), leeward heating increased with decreasing Reynolds number; the opposite was true for separated flow, which occurred when the fore-core angle of attack exceeded about 0.6-0.8 times the fore-cone half-angle. Leeward cross-flow separation first occurred just ahead of the base and moved upstream with increasing angle of attack. In general, windward heating was predicted to within 10% with a computer code that solves the steady, three-dimensional parabolized Navier-Stokes (PNS) equations. Although leeward heating distributions were predicted qualitatively by the PNS code for both values of Reynolds number, quantitative agreement was somewhat poorer than on the windward side. Windward heating measured on these same models in the Langley Expansion Tube in real (dissociated) air exceeded the present ideal-air values by about 30%; this difference was accounted for, to within engineering accuracy, using the viscous interaction parameter and the density ratio.

Acknowledgment

Gratitude is extended to V. T. Helms for obtaining the oil-flow patterns presented herein.

References

[1]Florence, D. E., "Aerothermodynamic Design Feasibility of a Mars Aerocapture/Aeromaneuver Vehicle," *Thermophysics of Atmospheric Entry*, edited by T.E. Horton, Progress in Astronautics and Aeronautics, Vol. 82, AIAA, New York, 1982, pp. 477-519.

[2]Florence, D. E., "Aerothermodynamic Design Feasibility of a Generic Planetary Aerocapture/Aeromaneuver Vehicle," AIAA Paper 81-1127, June 1981.

[3]Walberg, G. D., "A Survey of Aeroassisted Orbit Transfer," *Journal of Spacecraft and Rockets*, Vol. 22, March-April 1985, pp. 3-18.

[4]Miller, C. G. and Gnoffo, P. A., "Pressure Distributions and Shock Shapes for 12.84°/7° On-Axis and Bent-Nose Biconics in Air at Mach 6," NASA TM 83222, Dec. 1981.

[5]Miller, C. G. and Gnoffo, P. A., "An Experimental Investigation of Hypersonic Flow Over Biconics at Incidence and Comparison to Prediction," AIAA Paper 82-1382, Aug. 1982.

[6]Miller, C. G., Blackstock, T. A., Helms, V. T., and Midden, R. E., "An Experimental Investigation of Control Surface Effectiveness and Real-Gas Simulation for Biconics," AIAA Paper 83-0213, Jan. 1983.

[7]Miller, C. G., Gnoffo, P. A., and Micol, J. R., "Laminar Heat Transfer Distributions on Biconics at Incidence in Hypersonic-Hypervelocity Flows," NASA TP 2213, 1984.

[8]Gnoffo, P. A., "Hypersonic Flows Over Biconics Using a Variable-Effective-Gamma, Parabolized-Navier-Stokes Code," AIAA Paper 83-1666, July 1983.

[9]Miller, C. G., "Comparison of Thin-Film Resistance Heat-Transfer Gages with Thin-Skin Transient Calorimeter Gages in Conventional Hypersonic Wind Tunnels," NASA TM 83197, Dec. 1981.

[10]Miller, C. G., "Measured Pressure Distributions, Aerodynamic Coefficients, and Shock Shapes on Blunt Bodies at Incidence in Hypersonic Air and CF_4," NASA TM 84489, Sept. 1982.

[11]Fay, J. A. and Riddell, F. R., "Theory of Stagnation Point Heat Transfer in Dissociated Air," *Journal of the Aeronautical Sciences*, Vol. 25, Feb. 1958, pp. 73-85, 121.

[12]Vigneron, Y. C., "Calculation of Supersonic Viscous Flow Over Delta Wings with Sharp Subsonic Leading Edges," AIAA Paper 78-1137, July 1978.

[13]Agarwal, R. and Rakich, J. W., "Supersonic Laminar Viscous Flow Past a Cone at Angle of Attack in Spinning and Coning Motion," *AIAA Journal*, Vol. 20, June 1982, pp. 761-768.

[14]Gnoffo, P. A., "A Vectorized, Finite-Volume, Adaptive Grid Algorithm Applied to Planetary Entry Problems," AIAA Paper 82-1018, June 1982.

[15]Stetson, K. F., "Boundary-Layer Separation on Slender Cones at Angle of Attack," *AIAA Journal*, Vol. 10, May 1972, pp. 642-648.

[16]Stetson, K. F., "Effect of Bluntness and Angle of Attack on Boundary Layer Transition on Cones and Biconic Configurations," AIAA Paper 79-0269, Jan. 1979.

[17]Dearing, D. J., "Laminar Heat-Transfer Distributions for a Blunted-Cone, Cone-Frustum Reentry Configuration at Mach 10," NASA TN D-5146, April 1969.

[18]Marchand, E. O., Lewis, C. H., and Davis, R. T., "Second-Order Boundary Layer Effects on a Slender Blunt Cone at Hypersonic Conditions," AIAA Paper 68-54, Jan. 1968.

[19]Widhopf, G. F., "Turbulent Heat-Transfer Measurements on a Blunt Cone at Angle of Attack," *AIAA Journal*, Vol. 9, Aug. 1971, pp. 1574-1580.

[20]Rakich, J. V., "Iterative PNS Method for Attached Flows with Upstream Influence," AIAA Paper 83-1955, July 1983.

[21]Swaminathan, S., Kim, M. D., and Lewis, C. H., "Real Gas Flows Over Complex Geometries at Moderate Angles of Attack," AIAA Paper 82-0392, Jan. 1982.